Atmospheric
Measurement
Techniques

A method for colocating satellite X_{CO_2} data to ground-based data and its application to ACOS-GOSAT and TCCON

H. Nguyen[1], G. Osterman[1], D. Wunch[2], C. O'Dell[3], L. Mandrake[1], P. Wennberg[2], B. Fisher[1], and R. Castano[1]

[1]Jet Propulsion Laboratory, California Institute of Technology, Pasadena, CA, USA
[2]California Institute of Technology, Pasadena, CA, USA
[3]Colorado State University, Fort Collins, CO, USA

Correspondence to: H. Nguyen (hai.nguyen@jpl.nasa.gov)

Abstract. Satellite measurements are often compared with higher-precision ground-based measurements as part of validation efforts. The satellite soundings are rarely perfectly coincident in space and time with the ground-based measurements, so a colocation methodology is needed to aggregate "nearby" soundings into what the instrument would have seen at the location and time of interest. We are particularly interested in validation efforts for satellite-retrieved total column carbon dioxide (X_{CO_2}), where X_{CO_2} data from Greenhouse Gas Observing Satellite (GOSAT) retrievals (ACOS, NIES, RemoteC, PPDF, etc.) or SCanning Imaging Absorption SpectroMeter for Atmospheric CHartographY (SCIAMACHY) are often colocated and compared to ground-based column X_{CO_2} measurement from Total Carbon Column Observing Network (TCCON).

Current colocation methodologies for comparing satellite measurements of total column dry-air mole fractions of CO_2 (X_{CO_2}) with ground-based measurements typically involve locating and averaging the satellite measurements within a latitudinal, longitudinal, and temporal window. We examine a geostatistical colocation methodology that takes a weighted average of satellite observations depending on the "distance" of each observation from a ground-based location of interest. The "distance" function that we use is a modified Euclidian distance with respect to latitude, longitude, time, and midtropospheric temperature at 700 hPa. We apply this methodology to X_{CO_2} retrieved from GOSAT spectra by the ACOS team, cross-validate the results to TCCON X_{CO_2} ground-based data, and present some comparisons between our methodology and standard existing colocation methods showing that, in general, geostatistical colocation produces smaller mean-squared error.

1 Introduction

Carbon dioxide (CO_2) is an important anthropogenic greenhouse gas, and quantifying the exchange of CO_2 between the atmosphere and the Earth's surface is a critical part of the global carbon cycle and an important determinant of future climate (Gruber et al., 2009). One important measure of CO_2 is total column carbon dioxide (X_{CO_2}), which is available from ground-based Total Carbon Column Observing Network (TCCON; Wunch et al., 2011a) and from space-based satellite instruments such as the Greenhouse gases Observing Satellite (GOSAT; Yokota et al., 2004; Hamazaki et al., 2005) and the SCanning Imaging Absorption SpectroMeter for Atmospheric CHartographY (SCIAMACHY; Bovensmann et al., 1999).

Ground-based total column CO_2 measurements tend to be more precise and accurate than space-based measurements, but ground-based stations often are sparsely located around the globe, and areas such as Siberia, Asia, Africa, South America, and the oceans have particularly poor coverage. Satellite instruments have much better coverage and are able to sample the entire globe in a matter of days or weeks. Together, the ground-based and space-based CO_2-observing instruments provide a complementary ensemble of high-precision, sparse-coverage and lower-precision, global-coverage measurements. An important component of satellite retrieval assessment is validation relative to independent in situ ground-based sources of data in order to assess important metrics such as bias and variability relative to the underlying true process. These bias and variability assessments can in turn be used to improve the retrieval algorithm to reduce spurious error resulting from factors such as limited

understanding of the instrument's calibration, uncertainties in the O_2 and CO_2 absorption cross sections, and subtle errors in the implementation of the retrieval algorithm (Crisp et al., 2012).

Often, there are spatial and temporal mismatches in the observed locations of the remote sensing instrument and ground-based validation instrument, and some spatial (and temporal) interpolation is required in order to "colocate" the two sources of data before a direct comparison is possible. We define "validation colocation" as estimating, through interpolation using nearby satellite observations, what a remote sensing instrument would have seen at a certain chosen location and time. In this paper, we examine a new colocation methodology that is mathematically motivated in an error-minimization framework. Specifically, we are interested in developing a colocation methodology to combine retrieved X_{CO_2} data from GOSAT spectra using the Atmospheric CO_2 Observations from Space (ACOS) for comparison against TCCON X_{CO_2} data with the goal of minimizing the expected interpolation error.

Colocation methods for X_{CO_2} in the existing literature include geographical, T_{700} (Wunch et al., 2011b), and model-based (Guerlet et al., 2013) colocation. Geographical colocation typically defines a spatiotemporal neighborhood region, also known as a coincidence criterion, around the location of interest and then take summary statistics (e.g., mean or median). Examples of geographical colocation includes averaging all same-day satellite observations falling within $\pm 5°$ of a location of interest (Inoue et al., 2013), averaging all observations falling within $5°$ and $\pm 2\,h$ (Cogan et al., 2012), and taking the monthly median of all observations within a $10° \times 10°$ lat–long box (Reuter et al., 2013).

More sophisticated colocation methodologies add other correlated geophysical covariates in constructing such "neighborhoods" under the principle that conditioning on these additional correlated covariates would improve the quality of the comparison. Wunch et al. (2011b)'s T_{700} colocation method takes the average of all GOSAT observations falling within $\pm 30°$ longitude, $\pm 10°$ latitude, ± 5 days, and ± 2 kelvin in T_{700} of the TCCON location of interest. Guerlet et al.'s model-based method similarly takes the average of all same-day satellite values that fall within $\pm 7.5°$ latitude, $\pm 25°$ longitude, and ± 0.5 ppm of the 3-day-averaged model X_{CO_2} data.

All the colocation methodologies above operate on an implicit assumption that observations "near" one another are more likely to be correlated, where "nearby" indicates being proximal in a coordinate space and metric. The notion of "nearness" is captured in the definition of "neighborhood" that they specify; however, all observations falling within such a neighborhood are given equal weights in the computation of the summary statistics. While this approach might be intuitive and straightforward, it fails to take further advantage of the spatial information encoded within the coincident locations. For instance, suppose that we have 10 satellite observations falling within a coincident neighborhood of a ground-based station. The colocation methods above do not distinguish between the case where we have 10 satellite observations retrieved exactly at the ground-based station and the case where the 10 observations are retrieved far away on the edge of the neighborhood region; the colocation methods would return the same colocated value in both cases.

In this paper, we present a refinement of these colocation methodology by modeling the correlation structure as a function of "distance" using geostatistics, and then weighting nearby satellite observations by their correlation with one another and correlation with the location of interest. Our geostatistical methodology is motivated under an error-minimization mathematical framework and is related to optimal interpolation (for more detail, see kriging in Cressie, 1993, Chapter 2). Our methodology has the same framework as Zeng et al. (2014), although they applied the methodology in the context of gap-filling CO_2 from regional data and not for defining colocation criteria, and they did not consider the addition of non-spatial and non-temporal covariates in their model.

The benefits of a geostatistical approach include explicit specification of the underlying covariance structure, error propagation, and minimized expected mean-squared error. All colocation methodologies are essentially interpolation techniques, which result in an interpolation uncertainty that is incorporated into the variability of the colocated/validation data comparison. It is important to minimize the interpolation error so that we can better assess the underlying variability and bias between the satellite and validation data. The geostatistical colocation methodology has the attractive theoretical property that, given the correct spatial correlation structure, it has the lowest interpolation error of all linear methodologies.

In Sect. 2, we describe the data from ACOS-GOSAT and TCCON. Section 3 contains the details of our methodology as well as the estimation procedure, and we compare the performance of our geostatistical methodology to existing colocation methods in Sect. 4. Summary and discussion of the methodology along with possible extensions are presented in Sect. 5.

2　Overview of ACOS-GOSAT, TCCON, and auxiliary data sources

GOSAT was launched on 23 January 2009 as a joint venture by the National Institute for Environmental Studies (NIES), the Japanese Space Agency (JAXA), and the Ministry of the Environment (MOE). It is a polar-orbiting satellite dedicated to the observation of total-column CO_2 and CH_4, both major greenhouse gases, from space using reflected sun-light spectra from the Thermal And Near-infrared Sensor for carbon Observation Fourier transform spectrometer (TANSO-FTS; Hamazaki et al., 2005). It flies at approximately 665 km

altitude, and it completes an orbit every 100 min. The satellite returns to the same observation location every 3 days (Morino et al., 2011).

Following the failure of the Orbiting Carbon Observatory (OCO) launch in February 2009, the OCO project formed the Atmospheric CO_2 Observations from Space (ACOS) task and, under agreement with NIES, JAXA, and MOE, applied the OCO retrieval algorithm to the GOSAT spectra to compute column-averaged dry-air mole fractions of CO_2. The ACOS-GOSAT data processing algorithm is based on the optimal estimation approach of Rodgers (2000) and is described in detail in O'Dell et al. (2012). It is modified from the OCO retrieval algorithm (Bosch et al., 2006; Connor et al., 2008; Boesch et al., 2011) to account for the different physical viewing geometries and properties such as instrument line shapes and noise models.

In this paper, we assess the performance of different colocation methods on ACOS-GOSAT data by comparing colocated values to the more precise and accurate TCCON data. We use the v3.3 release of ACOS-GOSAT data, available from the Goddard Data and Information Services Center spanning July 2009 to April 2013 (see ACOS Data Access in the References for notes). GOSAT data are divided into three categories: glint (ocean) data, land high (H)-gain data, and land medium (M)-gain data. The v3.3 data user's guide notes that M-gain data and ocean glint data have some deficiencies in that particular version and should only be used with heightened caution (Osterman et al., 2013). Hence in this paper we only make use of H-gain land data.

Following the recommendation of the data user's guide, we screen the v3.3 H-gain data using a set of 11 criteria to obtain data suitable for scientific analysis. The set of screening criteria is reproduced in Table 5. The ACOS-GOSAT data have a bias that is known to be correlated with certain other variables such as air mass, blended albedo, and posterior–prior surface pressure difference (Wunch et al., 2011b). The v3.3 data user's guide recommends a linear bias correction to ACOS-GOSAT X_{CO_2} based on the difference between the retrieved and prior surface pressure from the A-band cloud screen and the ratio of the signal in the strong CO_2 band to that of the $O_2 A$ band (Osterman et al., 2013). However, since such bias correction was done through comparison of v3.3 ACOS retrievals with models and TCCON retrievals, we refrain from applying the v3.3 bias correction to avoid potential "feedback" in the comparison of our colocated v3.3 ACOS and TCCON values.

TCCON consists of ground-based Fourier transform spectrometers that record direct solar spectra in the near infrared. These spectra are then used to retrieve column-averaged abundances of atmospheric constituents, including CO_2, CH_4, N_2O, HF, CO, and H_2O, which are directly comparable with the near-infrared total-column measurements from space-based instruments (Wunch et al., 2011a). Whereas GOSAT retrievals are susceptible to variability resulting from contamination by optically thick clouds and aerosols that were missed by the cloud-screening process (O'Dell et al., 2012), TCCON directly observes the solar disk and hence is less sensitive to errors from scattered light (Crisp et al., 2012).

TCCON sites sample in a diverse range of atmospheric states, which include tropical and polar regions, continental and maritime, polluted and clean, providing valuable validation link between space-based measurements and the extensive ground-based in situ network (Wunch et al., 2011a). TCCON X_{CO_2} data in turn are validated against integrated aircraft profiles (Washenfelder et al., 2006; Deutscher et al., 2010; Messerschmidt et al., 2011; Wunch et al., 2010) and have a precision and accuracy of ~ 0.8 ppm (Wunch et al., 2010).

We use the 2012 release version of the TCCON data ("GGG2012") from the TCCON Data Archive (see TCCON Data Access in the References for more information) for the following 16 locations: Bialystok, Bremen, Darwin, Eureka, Garmisch, Izaña, Karlsruhe, Lamont, Lauder (both 120HR and 125HR), Ny-Ålesund, Orleans, Park Falls, Reunion, Sodankyla, Tsukuba (both 120HR and 125HR), and Wollongong. At each TCCON location, we use all available data that fall within the period of July 2009 to April 2013. A map of the TCCON locations is shown in Fig. 1. This particular version of TCCON data suffered from site-to-site biases due to a laser sampling issue inside the Bruker 125HR instruments, and thus we corrected for these biases using the TCCON recommended bias corrections (for more detail, see TCCON Data Access, 2013).

Atmospheric variability of X_{CO_2} has been shown to be correlated to the free-tropospheric potential temperature, which can be considered as a proxy for equivalent latitude for X_{CO_2} in the Northern Hemisphere (Keppel-Aleks et al., 2011). In this paper, we follow Wunch et al. (2011b) in making use of midtropospheric temperature as one of the covariates along with latitude, longitude, and time. Specifically, we use the midtropospheric temperature field at 700 hPa from the National Centers for Environmental Prediction and the National Center for Atmospheric Research (NCEP/NCAR) reanalysis product, which uses a frozen state-of-the-art analysis/forecast system and performs data assimilation using past data (Kalnay et al., 1996). The midtropospheric temperature field at 700 hPa should be directly proportional to the potential temperature at 700 hPa for the range of temperature of interest, and its inclusion as a covariate should allow us to construct better colocation metrics.

2.1 Averaging kernel correction

To compare two observations obtained through optimal estimation properly, the retrievals must be computed around a common a priori profile and the averaging kernels must be applied to account for the effect of smoothing (Rodgers and Connor, 2003). A detailed exposition on applying the averaging kernel correction for a ACOS-GOSAT and TCCON

Table 1. Annual and seasonal trend coefficients.

	Intercept (ppm)	Slope (ppm year^{-1})	Amplitude (ppm)	Phase shift (radian)
Northern Hemisphere	385.7900	2.6061	3.2040	0.1556
Southern Hemisphere	383.5127	2.4878	0.3099	4.0978
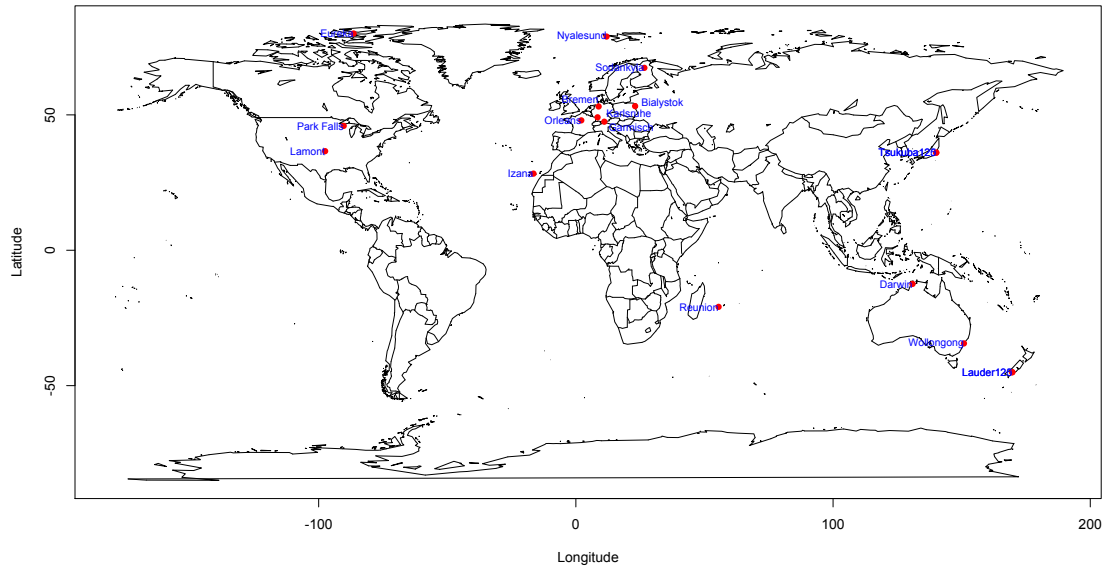
Figure 1. Map showing the 16 TCCON locations for which we perform GOSAT/ACOS and TCCON colocation comparison.

comparison is given in Sect. 4 and Appendix A of Wunch et al. (2011b).

Typically, to compare retrieval results from two different instruments with different viewing geometrics, retrieval algorithms, a priori profiles (x_a), and averaging kernel ($\mathbf{A}$), we need an common ensemble profile (x_c) and covariance matrix ($\mathbf{S}_c$); these represent the mean and variability of the atmosphere at the common comparison location. As an alternative, we can use one observing system to try to retrieve what the other system would have produced as its retrieved total column (Rodgers and Connor, 2003). Given that TCCON retrievals are considered more precise and accurate, we smooth the TCCON value with the ACOS-GOSAT column averaging kernels to produce what ACOS-GOSAT would have produced at the TCCON location given the TCCON profile as "truth".

Fortunately, ACOS v3.3 a priori profiles and TCCON a priori profiles are very similar to one another, and hence we only need to account for differences in the averaging kernels. We use the following averaging kernel equation from Appendix A of Wunch et al. (2011b):

$$\hat{z}_{12} = z_a + (\gamma - 1) \sum_j h_j a_{1j} x_{aj}, \tag{1}$$

where z_a is the a priori X_{CO_2}; $\hat{z}_i$ is the retrieved X_{CO_2}, with $i = 1$ for ACOS and $i = 2$ for TCCON; h is the X_{CO_2}

pressure weighting function; and a is the X_{CO_2} averaging kernel norm. The term γ is a scaling factor that produces the best fit of the TCCON output to the spectrum, and it is approximated as a ratio between the retrieved TCCON X_{CO_2} and the a priori X_{CO_2},

$$\gamma \approx \frac{\hat{z}_2}{z_a}.$$

We apply Eq. (1) to TCCON data between July 2009 and April 2013 at the 16 chosen TCCON locations. For each TCCON observation, we obtain the corresponding ACOS a priori information using the colocation neighborhood region defined in Wunch et al. (2011b); see Sect. 4 for more detail. Figure 2 displays a plot of the relationship between the original TCCON retrievals versus the averaging-kernel-corrected TCCON data. In effect, the averaging kernel correction tends to pull TCCON observations closer to the ACOS a priori X_{CO_2}; TCCON values that are higher than the ACOS a priori value tend to be pulled downwards, while TCCON values lower than the ACOS a priori X_{CO_2} tend to be pulled upwards. The standard deviation of the difference between non-corrected and corrected TCCON values, aggregated over all TCCON sites, is 0.24 ppm.

Having done averaging kernel correction to put the TC-CON and ACOS retrievals on the same footing, in the next section we describe our methodology for optimally colocating ACOS-GOSAT observations to any TCCON location. The colocated values will then be compared to averaging-kernel-corrected TCCON data in Sect. 4.

3 Geostatistical colocation

Our colocation methodology exists within a geostatistical framework, which is a part of the broader area of spatial statistics. Here, we briefly review that framework, give some necessary notation, and present basic derivations for estimation in a spatial context.

Let $\{Y(s) : s \in D\}$ be a hidden, real-valued spatial process on a multidimensional domain. In the application of ACOS-GOSAT and TCCON, we let $s = (s_{lat}, s_{lon}, s_t, s_T)'$ be a four-dimensional vector, specifying the latitude in degrees, longitude in degrees, time in fractional days, and midtropospheric temperature in kelvin at 700 hPa (T_{700}), respectively, and we assume $Y(s)$ is the X_{CO_2} process at location s. We assume that the $Z(s)$, X_{CO_2} retrieval at location s, is a sum of the true X_{CO_2} process and a retrieval-error term; that is,

$$\begin{aligned} Z(s) &= Y(s) + \epsilon(s) \\ &= t(s) + \nu(s) + \epsilon(s), \end{aligned} \quad (2)$$

where $t(s)$ is a large-scale deterministic trend term that accounts for seasonal and yearly trends, $\nu(s)$ is a small-scale variability term that accounts for spatial correlation, and $\epsilon(s)$ is the retrieval-error term. We also assume that we have a variogram function $2\gamma(s_i, s_j)$, which describes the degree of spatial dependence between any two locations s_i and s_j as in the following definition:

$$2\gamma(s_i, s_j) = \text{var}(Z(s_i) - Z(s_j)) =$$
$$\mathbf{E}\left(|(Z(s_i) - t(s_i)) - (Z(s_j) - t(s_j))|^2\right); \; s_i, s_j \in D. \quad (3)$$

Let $\mathbf{Z} = (Z(s_1), Z(s_1), \ldots, Z(s_N))'$ be the vector of satellite observations taken at N footprints around an interpolation point s_0, and let $\mathbf{T} = (t(s_1), t(s_1), \ldots, t(s_N))'$ be the corresponding N-dimensional vector of trend terms. We wish to find an estimate of $Y(s_0)$ as a linear combination of the de-trended retrieved X_{CO_2} vector $\mathbf{D} = (\mathbf{Z} - \mathbf{T})$ and an unknown vector of coefficients a'_{s_0}; that is,

$$\hat{Y}(s_0) = t(s_0) + a'_{s_0}\mathbf{D}, \quad (4)$$

such that we minimize the expected mean-squared error

$$\min_{a_{s_0}} \mathbf{E}\left((Y(s_0) - \hat{Y}(s_0))^2\right), \quad (5)$$

subject to the unbiasedness constraint $a'_{s_0}\mathbf{1} = 1$.

The solution to the constrained minimization problem in Eqs. (4) and (5) can be found using the method of Lagrange multipliers. Cressie (1993) gives the following equation for the solution a_{s_0} that satisfies Eq. (4) and (5),

$$\begin{pmatrix} a_{s_0} \\ \lambda \end{pmatrix} = \quad (6)$$
$$\begin{pmatrix} \gamma(s_1, s_1) & \cdots & \gamma(s_1, s_N) & 1 \\ \vdots & \ddots & \vdots & \vdots \\ \gamma(s_N, s_1) & \cdots & \gamma(s_N, s_N) & 1 \\ 1 & \cdots & 1 & 0 \end{pmatrix}^{-1} \begin{pmatrix} \gamma(s_1, s_0) \\ \vdots \\ \gamma(s_N, s_0) \\ 1 \end{pmatrix},$$

where λ is the scalar Lagrange multiplier and a_{s_0} is the vector of kriging coefficient.

An attractive property of the geostatistical approach is that the semivariogram function can be used to calculate the expected estimation error at the interpolation location. The expression for the interpolation error is as follows:

$$\hat{\sigma}(s) = \begin{pmatrix} a'_{s_0} & \lambda \end{pmatrix} \begin{pmatrix} \gamma(s_1, s_0) \\ \vdots \\ \gamma(s_N, s_0) \\ 1 \end{pmatrix}. \quad (7)$$

Estimating the fully general semivariogram model $\gamma(s_N, s_0)$ is a difficult problem that is prone to robustness issues when the data are sparse. To make the problem more tractable, we assume that the variogram structure of $\mathbf{Z}$ is isotropic under certain distance metrics. In other words, we assume that the semivariogram capturing the spatial dependence between any two locations $\gamma(s_i, s_j)$ is only dependent on its "distance" as in the following equation:

$$\gamma(s_i, s_j) = \gamma(|s_i - s_j|_B), \quad (8)$$

where $|\cdot|_B$ is a modified Euclidean distance given by

$$|s_i - s_j|_B = \quad (9)$$

$$\sqrt{\left(\frac{(s_{i,lat} - s_{j,lat})^2}{B_1} + \frac{(s_{i,lon} - s_{j,lon})^2}{B_2} + \frac{(s_{i,t} - s_{j,t})^2}{B_3} + \frac{(s_{i,T} - s_{j,T})^2}{B_4}\right)}$$

$$= \sqrt{\left((s_i - s_j)'\mathbf{B}(s_i - s_j)\right)}, \quad (10)$$

and $\mathbf{B}$ is a diagonal 4×4 matrix whose diagonal elements $(1/B_1, 1/B_2, 1/B_3, 1/B_4)$ represent the scaling parameters along each of the coordinate directions: latitude, longitude, time, and T_{700}.

3.1 Application to ACOS-GOSAT and TCCON data

Computation of the colocated values and their corresponding interpolation error in Eqs. (4) and (7) requires that we know the trend $t(\cdot)$, the scaling diagonal matrix $\mathbf{B}$, and the semivariogram function $\gamma(\cdot, \cdot)$. In practice, these terms are unknown.

For our application, we will assume certain parametric forms for the trend $t(\cdot)$ and the semivariogram function $\gamma(\cdot, \cdot)$ and estimate the corresponding parameters along with $\mathbf{B}$ from the retrieved data.

Unfortunately, ACOS-GOSAT data are quite sparse once we pass the radiances through a cloud filter, retrieval selection criteria, and post-retrieval data quality filters. The relative global sparseness of the ACOS-GOSAT data makes it difficult to obtain robust estimates of the scaling matrix $\mathbf{B}$ and the semivariogram function $\gamma(\cdot, \cdot)$. We address this problem by using CarbonTracker model X_{CO_2} data to estimate these spatial–temporal dependence parameters. Our assumption here is that CarbonTracker and ACOS-GOSAT share the same medium- to large-scale spatiotemporal dependence structure for X_{CO_2}. For instance, the dynamics in Carbon-Tracker should reasonably approximate synoptic- and large-scale dependence in moderately homogeneous areas such as the Southern Hemisphere. Note that this assumption is not as restrictive as the assumption that CarbonTracker and ACOS-GOSAT have the same expected value of X_{CO_2} at every location.

CarbonTracker is a CO_2 assimilation system developed by the National Oceanic and Atmospheric Administration (NOAA) to keep track of the global CO_2 emissions and uptake. The model combines surface air samples collected around the globe and from tall towers and small aircraft in North America with an atmospheric transport model coupled with a Kalman filter to produce estimates of atmospheric CO_2 mole fractions on a global grid (Peters et al., 2007). The model X_{CO_2} data are regularly gridded at $1° \times 1°$ daily resolution, making it particularly convenient for use in spatial parameter estimation. We use 2 years' worth of Carbon-Tracker data (CT2001_oi) between January 2009 and December 2010 in estimating the trend $t(\cdot)$, the scaling matrix $\mathbf{B}$ and the semivariogram function $\gamma(\cdot, \cdot)$.

3.2 Trend terms

The trend term $t(\cdot)$ is a deterministic term that accounts for the annual increase in X_{CO_2} as well as the seasonal variations. This deterministic trend needs to be modeled, estimated, and removed from the data in Eq. (2) before we can apply the geostatistical colocation on the remaining stochastic terms in Eq. (4). We assume that the trend term in Eq. (4) can be modeled as a mixture of a linear constant trend and a seasonal sinusoidal trend,

$$t(s) = c_0(s) + c_1(s)s_t + a(s) \cdot \sin(2\pi s_t + \theta(s)), \qquad (11)$$

where $c_0(s)$ is the y intercept and $c_1(s)$ the slope of the linear portion, $a(s)$ is the amplitude of the seasonal sinusoidal variability, and $\theta(s)$ is the sinusoidal phase shift. The period for seasonal variability is assumed to be 1 year, and s_t is the time as a year fraction starting at 0 for 1 January 2009.
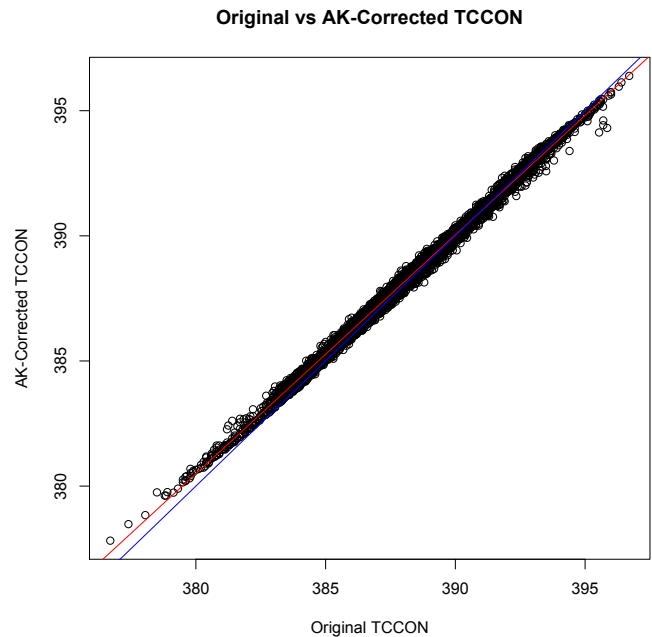
Figure 2. Matched TCCON original daily median observations vs. averaging-kernel-corrected TCCON values. The red line is the linear regression line, while the blue is the 1 : 1 line.

We make a simplifying assumption that the annual and seasonal trends are constant over the hemispheres. We aggregate daily CarbonTracker X_{CO_2} values over both the Northern and Southern Hemisphere for the entire 2-year period, and we compute the trend coefficients $\{c_0(s), c_1(s), a(s), \theta(s)\}$ using variable transformation and linear regression (Artis et al., 2007). The resulting coefficients are displayed in Table 1.

Table 1 indicate that the Northern Hemisphere tends to have higher X_{CO_2} than the Southern Hemisphere. The intercept term is higher for the Northern Hemisphere, indicating that the base X_{CO_2} there is higher, and the slope is marginally higher as well (2.61 vs. 2.49 ppm year^{-1}), indicating that the Northern Hemisphere has a higher rate of X_{CO_2} increase. The main differences between the hemispheres are the amplitudes and the phase shifts of the seasonal terms. CarbonTracker indicates that the Northern Hemisphere has a seasonal variability with an amplitude of 3.2 ppm, while the Southern Hemisphere has a much lower seasonal amplitude of 0.31 ppm. The phase shifts (0.16 vs. 4.10) differ by about half a year, which is consistent with the opposite seasons in the hemispheres.

A plot of the sinusoidal fits versus the aggregated data is shown in Fig. 3. In general, the sinusoidal curves roughly reproduce the linear trend and seasonal variability in the averaged CarbonTracker data. The fit is not perfect, and the difference between the two might be due to small-scale spatial variability, which will be captured in the remaining stochastic terms in Eq. (4).
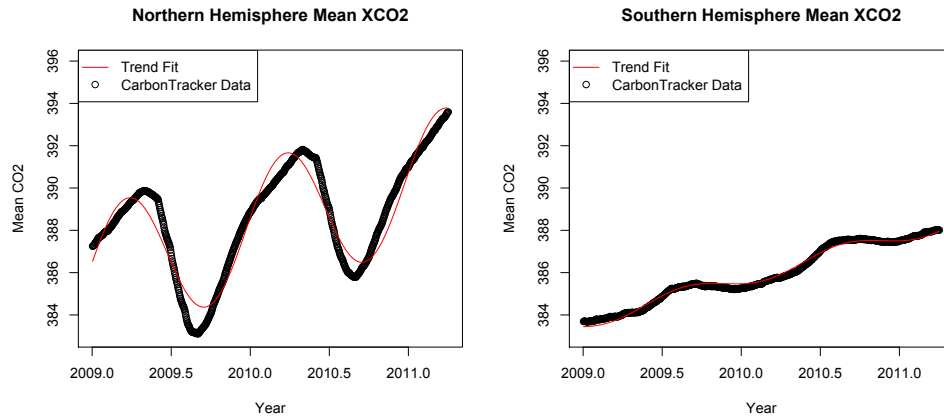
Figure 3. Plots of averaged CarbonTracker trend versus sinusoidal trend fit for the Northern Hemisphere (left) and Southern Hemisphere (right).

3.3 Parameter estimation

Having modeled and estimated the trend term $t(\cdot)$, we now estimate the scaling matrix $\mathbf{B}$ and the semivariogram function $\gamma(\cdot, \cdot)$. We model the semivariogram function with the spherical semivariogram, which has the form

$$\gamma(s_i, s_j) \equiv \gamma(h) =$$
$$(s - n)\left(\left(\frac{3h}{2r} - \frac{h^3}{2r^3}\right)\mathbf{1}_{(0,r)}(h) + \mathbf{1}_{[r,\infty)}(h)\right) + n, \quad (12)$$

where $h = |s_i - s_j|_B$ is the modified Euclidean distance between s_i and s_j; $\mathbf{1}_S(h)$ is 1 if $h \in S$, and 0 otherwise, the term n is the nugget, which denotes the height of the semivariogram at the origin where $h = 0$; the term s is called the sill, which is the limit of the semivariogram as $h \to \infty$; and r is the range, which is the distance at which the difference between the semivariogram and the sill is negligible (see Cressie, 1993, for more detail).

Given the scaling matrix $\mathbf{B}$, we can estimate the semivariogram parameters $\{n, s, r\}$ by constructing the robust empirical semivariogram estimator discussed in Cressie (1980) and Cressie (1993, Sect. 2.4) from the CarbonTracker data as follows. For $h > 0$, define

$$2\bar{\gamma}(h) \equiv \frac{\left\{\frac{1}{|N(h)|}\sum_{N(h)} |D(s_m) - D(s_n)|^{\frac{1}{2}}\right\}^4}{0.457 + \frac{0.494}{|N(h)|}}, \quad (13)$$

where $D(s)$ is the detrended CarbonTracker value at location s, and $N(h)$ is the set of observation pairs that are separated by a distance of h,

$$N(h) \equiv \{(s_n, s_m) : |s_n - s_m|_{B^*} = h; \quad m, n = 1, \dots, N\}.$$

In practice, the set $N(h)$ is defined using a small tolerance interval around h, since it may not be possible to find pairs of locations that are exactly distance h apart (Cressie, 1993, p. 70). The term $|N(h)|$ denotes the number of unique elements in $N(h)$.

We assume that the scaling matrix $\mathbf{B}$ and the semivariogram function $\gamma(\cdot, \cdot)$ are constant with respect to each hemisphere and with respect to time. To estimate the scaling matrix $\mathbf{B}$, we construct empirical semivariograms using data pairs that only approximately differ in one of the four coordinates. This effectively sets three of the four terms on the right-hand side of Eq. (9) to zero (or very close to zero), allowing us to estimate the single remaining scaling parameter, B_i. For instance, to estimate the scaling parameter along the longitudinal direction, we search through the CarbonTracker data for the corresponding hemisphere to obtain pairs of observations that share the same date, latitude, and T_{700} but different longitudes. We then calculate the robust semivariogram estimator in Eq. (13), compute the corresponding semivariogram fit to the spherical model in Eq. (12), and set the scaling parameter B_i equal to the resulting range r.

Table 2 contains the list of scaling parameters for the Northern Hemisphere and the Southern Hemisphere. In general, the scaling parameters agree fairly well with the coincidence windows given in Wunch et al. (2011b)'s T_{700} methodology. For the Northern Hemisphere, the scaling parameters for latitude, longitude, time, and T_{700} are 15.1, 24.5, 3, and 3.1, respectively; the corresponding parameters for the Southern Hemisphere are 11.6, 19.3, 3, and 2.3. This indicates that in general the Northern Hemisphere has longer spatial correlation range than the Southern Hemisphere.

Having estimated the scaling parameters $\mathbf{B}$, we construct a set of empirical semivariogram values using Eq. (13) for each of the hemispheres and estimate the semivariogram parameters $\{n, s, r\}$ using an iterative Gauss–Newton fitting algorithm to fit to the chosen spherical semivariogram model to the empirical semivariogram estimates (Cressie, 1985). The resulting nugget, sill, and range parameters for the Northern and Southern Hemisphere are presented in Table 2.

The nugget and the sill parameters indicate that in general the Northern Hemisphere has higher variability and that the spatial correlation structure is weaker in the Southern

Table 2. Scaling coefficients and semivariogram parameters for Eq. (9).

	B_1 (degrees)	B_2 (degrees)	B_3 (days)	B_4 (kelvin)	Nugget (n)	Sill (s)	Range (r)
Northern Hemisphere	15	25	3	3	0.3	2.3	1.98
Southern Hemisphere	11	19	3	2	0.21	0.73	1.7

Hemisphere. Having estimated the parameters for **B** and $\gamma(s_i, s_j)$, we can compute the colocated ACOS-GOSAT value at any TCCON location using Eqs. (4) and (6).

4 Comparison to existing methodologies

Having outlined the geostatistical colocation methodology in Sect. 3, we now assess its performance relative to existing methodologies, which include geographical colocation and Wunch et al. (2011a)'s T_{700} colocation. Our primary standard for comparison is the root-mean-squared error (RMSE) between TCCON and colocated ACOS-GOSAT data. This RMSE is the sum of the variability from various sources such as the underlying atmospheric variability, GOSAT and TCCON measurement errors, relative bias, and interpolation error resulting from colocation. In this experiment, we manipulate the magnitude of the interpolation error by varying the method of colocation. The resulting changes in total RMSE should be indicative of the corresponding changes in interpolation error.

Geographical colocation methodology is perhaps the most popular colocation methodology due to its simplicity and straightforwardness. Examples of geographical coincident criteria include selecting all same-day satellite observations falling within ±5° of a location of interest (Inoue et al., 2013), selecting data falling within ±30 min from about 0.5 to 1.5° rectangles centered at each validation site (Morino et al., 2011), selecting data within 5° and ±2 h (Butz et al., 2011; Cogan et al., 2012), selecting observations within a 10° × 10° lat–long box (Reuter et al., 2013), and selecting weekly data that fall within a 5° radius of a validation site (Oshchepkov et al., 2012). For the performance comparison in this section, we define a geographical colocation methodology by averaging all same-day satellite observations falling within 500 km of a location of interest. This colocation methodology is based on the one used in Inoue et al. (2013), with the exception that we replace the lat–long circle with a great-distance circle to avoid warping near the poles.

Wunch et al. (2011b) refined the geographical method by adding midtropospheric temperature at 700 hPa as an extra threshold to take advantage of the correlation between X_{CO_2} and midtropospheric temperature (Keppel-Aleks et al., 2011, 2012). Their colocation methodology locates and averages all ACOS-GOSAT observations falling within ±30° longitude, ±10° latitude, ±5 days, and ±2 kelvin in T_{700}. The

longitudinal constraint is reduced to ±10° for the Tsukuba TCCON site to avoid inordinate influence from ACOS-GOSAT retrievals over China. In this section, we assess the performance of Wunch et al. (2011b)'s colocation criterion and the geographical method relative to geostatistical colocation methodology between the period July 2009 and April 2013.

4.1 Comparison between ACOS-GOSAT and TCCON data

For the performance assessment, we use all available TCCON data from 16 locations (4 in the Southern Hemisphere, 12 in the Northern Hemisphere; see Fig. 1) between the period July 2009 and April 2013. Since the three colocation methodologies compute averages over large temporal spans, applying the three methodologies to individual same-station TCCON observations (which may be spaced seconds or minutes apart from one another) would result in a scenario where many temporally proximal TCCON observations are matched to the same ACOS-GOSAT colocated value. We avoid this problem by taking the daily median of TCCON X_{CO_2} values and using them as the standard against which we assess the outputs of the colocation methodologies.

Having taken the daily median of the TCCON X_{CO_2} values, we scan the entire TCCON data set and locate corresponding matches using the colocation methodologies. At every TCCON location and every day for which we have a daily median TCCON X_{CO_2} value, we gather the corresponding ACOS-GOSAT values falling within the respective coincidence regions and then compute the colocated value for each of the three methodologies. Some TCCON locations may not have a corresponding colocated ACOS-GOSAT value for particular days due to the fact that they do not have any GOSAT values within their coincidence neighborhood. The neighborhood regions are constructed separately for each TCCON location, and thus some ACOS-GOSAT sounding may be used more than once in computing the colocated values for several temporally or spatially proximal TCCON daily median values.

Figure 4 displays the colocated ACOS-GOSAT values versus the data from the 16 TCCON sites. The x axis displays the temporal range whereas the y axis displays the TCCON daily median values and the colocated ACOS-GOSAT from the three colocation methodologies. In general, the Wunch et al. (2011b) and geostatistical methodology have
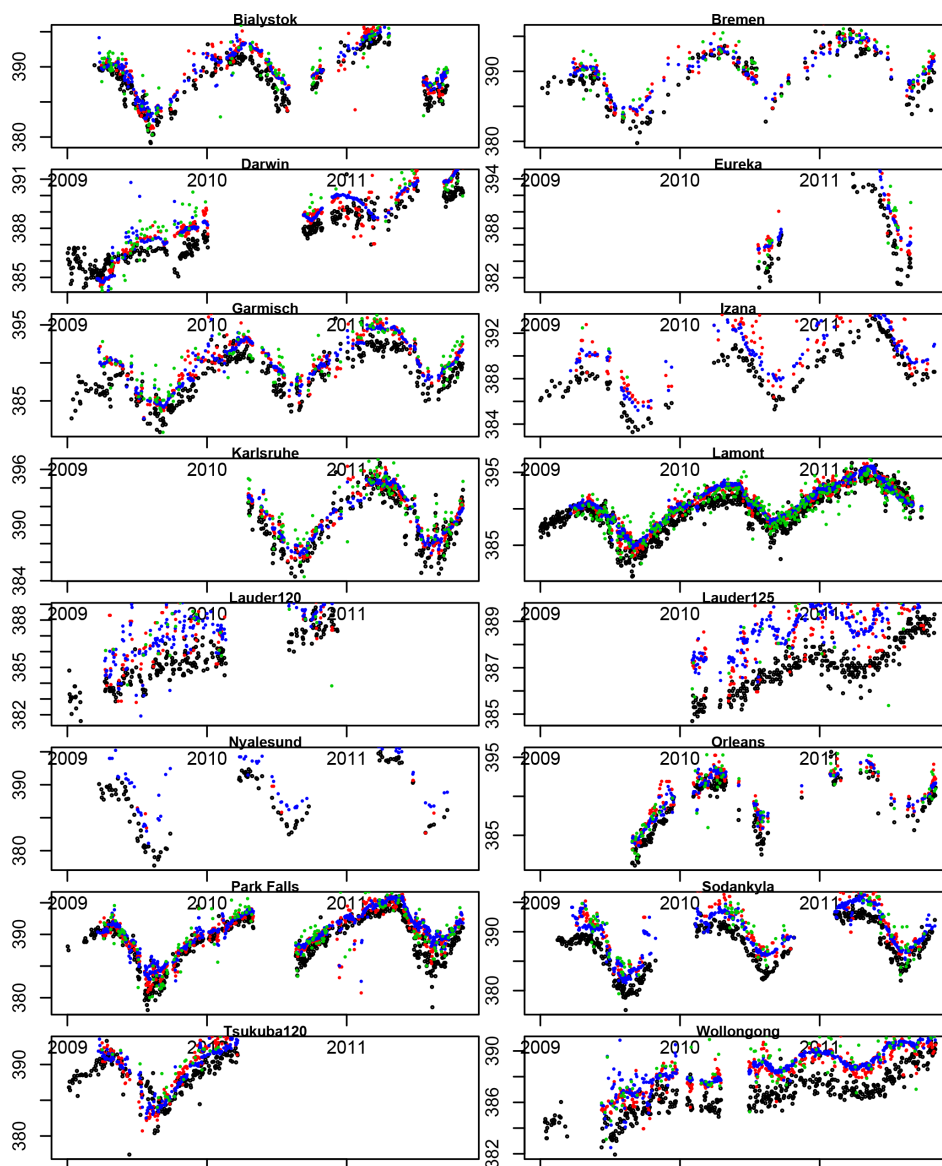
Figure 4. TCCON daily median (black) vs. T_{700} (red), geostatistical (blue), and geographical (green) colocation values. Time in days is displayed on the x axis, while X_{CO_2} concentration in ppm is displayed on the y axis. Reunion and Tsukuba125 data sets are omitted due to the low number of observations.

a lot more colocated values due the fact that they use data from a large spatiotemporal neighborhood surrounding a TC-CON site. From Fig. 4, all colocation methodologies indicate that ACOS-GOSAT X_{CO_2} tends to be larger than TC-CON X_{CO_2} and the magnitude of this bias is between 1 and 1.5 ppm. Northern TCCON sites such as Eureka and Ny-Ålesund do not have nearby ACOS-GOSAT H-gain good-quality retrievals during the winter due to ice and snow issues.

Table 4 displays five ACOS-GOSAT/TCCON summary statistics: number of matched days (N), mean bias, standard deviation, correlation coefficient (r), and slope. Geostatistical and T_{700} methodologies have wider coincidence

criteria than our chosen geographical methodology, and consequently have more daily matched ACOS-GOSAT/TCCON pairs. To better examine the patterns in Table 4, we display the main statistics (bias, standard deviation, and correlation coefficient) in graphical form in Fig. 5, with the TCCON stations listed in order of decreasing latitude.

In the top panel of Fig. 5, we examine the average bias between the three colocation methodologies versus TCCON daily median X_{CO_2} at each of the 18 TCCON data sets. The average bias is fairly consistent between the three methodologies and range between 0.6 and 2.5 ppm. In general, the T_{700} and geostatistical colocation methodologies tend to produce the same bias, while the geographical method has more

Table 3. Overall mean-squared error for the three colocation methodologies before and after averaging kernel (AK) correction on TCCON. Units are ppm.

	T_{700}	Geographical	Geostatistical
Before AK correction	1.57	1.88	1.43
After AK correction	1.45	1.60	1.22

Table 4. Overall summary statistics for the three colocation methodologies. Statistics include number of matched days (N), mean bias, standard deviation (SD), correlation coefficient (r), and slope.

		Geostatistical					T_{700}					Geographical				
Latitude	Location	N	mean	SD	r	slope	N	mean	SD	r	slope	N	mean	SD	r	slope
53.23	Bialystok	342	1.09	1.06	0.90	0.89	319	1.04	1.46	0.83	0.96	100	0.87	1.93	0.72	0.95
53.10	Bremen	185	0.67	1.33	0.86	0.78	167	0.85	1.51	0.81	0.83	66	0.92	1.65	0.77	0.86
−12.43	Darwin	325	0.39	0.87	0.79	1.05	302	0.28	0.99	0.76	1.11	84	0.80	1.10	0.81	1.22
80.05	Eureka	46	2.21	1.08	0.80	0.82	43	2.45	1.67	0.66	0.97	19	3.10	2.20	0.65	1.19
47.48	Garmisch	357	1.42	1.09	0.87	0.91	321	1.54	1.34	0.81	0.93	127	1.94	1.82	0.74	0.95
23.30	Izaña	156	1.58	0.89	0.88	0.96	144	1.90	1.14	0.82	0.99	3	3.37	0.50	0.95	0.99
49.10	Karlsruhe	246	0.63	1.11	0.86	0.81	233	0.64	1.20	0.83	0.83	109	1.00	1.61	0.73	0.83
36.60	Lamont	795	0.73	0.97	0.89	0.82	729	0.81	0.92	0.90	0.86	345	0.66	1.37	0.77	0.81
−45.05	Lauder120	146	1.12	1.22	0.53	0.99	136	1.23	1.53	0.38	0.91	31	1.24	1.95	0.16	0.62
−45.05	Lauder125	235	1.36	0.55	0.76	0.91	224	1.32	1.31	0.34	0.89	30	1.23	1.87	0.21	0.92
78.92	Ny-Ålesund	10	2.32	0.96	0.93	0.87	10	1.42	1.80	0.75	0.72					
47.97	Orleans	208	1.13	1.14	0.89	0.83	196	1.34	1.36	0.84	0.86	74	1.11	1.79	0.79	0.87
45.94	Park Falls	590	1.20	1.49	0.83	0.80	550	0.94	1.52	0.82	0.87	165	1.11	1.66	0.81	1.06
−20.90	Reunion	10	0.88	0.70	0.20	0.12	10	1.41	0.55	0.58	0.35					
67.37	Sodankyla	312	1.93	1.20	0.91	0.94	291	2.49	1.67	0.85	1.01	101	2.62	1.79	0.83	1.09
36.05	Tsukuba120	179	0.83	1.82	0.66	0.90	170	1.17	2.12	0.65	1.05	35	2.48	1.46	0.83	1.14
36.05	Tsukuba125	51	1.11	2.01	0	−0.03	49	2.31	2.37	0	−0	13	4.07	1.08	0.28	0.45
−34.41	Wollongong	437	1.32	0.85	0.70	0.81	404	1.22	0.95	0.64	0.81	115	1.79	1.38	0.51	0.88

pronounced variability in the estimates of mean bias at the TCCON sites. This is likely due to the fact that the geographical method has a much smaller neighborhood region, and thus does not yield enough colocated matches relative to TCCON to produce a robust bias estimate. All three methodologies tend to have high bias estimates for the three northernmost TCCON sites: Sodankyla, Eureka, and Ny-Ålesund. This is likely because soundings acquired over these snowy and icy surfaces have low reflectivity in the 1.61 and 2.06 μm bands; consequently scattering by thin clouds and aerosols can constitute a larger fraction of the total signal and introduce larger uncertainties in the optical path length (Crisp et al., 2012).

The clear delineating metric between the three methodologies is the RMSE (also known as standard deviation), which we display in the middle panel of Fig. 5 on a station-by-station basis. The three methodologies are roughly separated into clusters: the geographical method has on average the highest RMSE, T_{700} ranks in the middle, and geostatistical colocation has the lowest RMSE. One might expect the geographical method to have the lowest RMSE since it only accepts ACOS-GOSAT values within a fairly narrow spatiotemporal neighborhood (500 km same-day window). However, this is not the case since the RMSE is a function of both the spatial dependence structure *and* the retrieval error

characteristics. Since the GOSAT measurements tend to have relatively large single-sounding uncertainties, the T_{700} and the geostatistical colocation methods are able to take advantage of the large number of observations within the coincident neighborhood to reduce the variability through the law of large numbers.

While the T_{700} and the geostatistical methods tend to have the same mean bias (see top panel of Fig. 5), the geostatistical method tends to produce lower RMSE. Table 3 displays the overall RMSE aggregated over all TCCON locations for the three colocation methodologies using both original and averaging-kernel-corrected TCCON data. In both cases, the geostatistical methodology has the lowest RMSE while the geographical methodology has the highest. This is not surprising since the geostatistical method is explicitly motivated by the error-minimizing framework in Eq. (5). In other words, given that the spatial dependency structure that we learned from CarbonTracker is correct, the geostatistical methodology is guaranteed to produce the lowest root-mean-squared interpolation error relative to the truth (here represented by TCCON) of all linear methodologies. While it is unlikely that we have perfectly estimated the true spatial dependency structure of ACOS-GOSAT data from CarbonTracker, we note that the improvement in performance indicates that the dependency structure that we ultimately

Table 5. Advanced screening criteria for ACOS v3.3 L2 H-gain data (Osterman et al., 2013, Sect. 2.5.2).

Variable	Comment	Criteria
RetrievalResults/outcome_flag	Flag indicating full physics outcome	1 or 2
RetrievalResults/aerosol_total_aod	Retrieved total-column-integrated aerosol optical depth for all aerosol types	0.01 to 0.02
SoundingGeometry/sounding_altitude_stddev	Standard deviation of the measure of altitude of the surface within the sounding	< 200
IMAPDOASPreprocessing/CO2_ratio_idp	Ratio of retrieved CO_2 column (no scattering code) in weak and strong CO_2 band	0.995 to 1.015
IMAPDOASPreprocessing/H2O_ratio_idp	Ratio of retrieved H_2O column (no scattering code) in weak and strong CO_2 band	0.92 to 1.05
ABandCloudScreen/surface_pressure_delta_cld	Difference between surface pressure and a priori surface pressure	−825 to 575
SpectralParameters/reduced_chi_squared_O2_fph	The reduced χ^2 value of the O_2 A-band clear-sky fit used in determine the presence or absence of cloud	< 1.5
RetrievalResults/albedo_slope_strong_CO2	Retrieved spectral dependence of Lamberion component of albedo within strong CO_2 channel	$> -10.0 \times 10^{-5}$
RetrievalResults/albedo_slope_o2	Retrieved spectral dependence of Lamberion component of albedo within O_2 channel	$< -1.3 \times 10^{-5}$
Blended Albedo	A combination of two albedo terms	< 0.08

derived, compared to the other colocation methodologies in this section, is more reflective and representative of the true underlying dependence structure.

Another way to assess the fit between ACOS-GOSAT and TCCON values is through examining the correlation coefficient. Since the satellite and station instruments both observe total-column X_{CO_2}, we expect the two to follow a linear relationship with a slope of 1 and a y intercept equal to the mean bias. The correlation coefficient is a good tool to examine the strength and direction of the linear relationship between the ACOS-GOSAT and TCCON values, and we show the correlation estimates at each of the TCCON sites in the bottom panel of Fig. 5.

In our particular application, correlation values closer to 1 indicate stronger linear dependence. In this respect, geostatistical colocation performs marginally better than T_{700} colocation, and they both perform better than geographical colocation. The correlation estimates mostly cluster within the range of 0.75 to 0.99, with the exception being TCCON stations in the Southern Hemisphere. This likely results from the fact that the Northern Hemisphere and the Southern Hemisphere have a different seasonal and synoptic variability ratio. In general, the ACOS-GOSAT retrievals do quite well in capturing the overall seasonal trends in both hemispheres. However, in the Northern Hemisphere, the seasonal variability amplitude is larger than the synoptic variability, and consequently the correlation coefficient between ACOS-GOSAT and TCCON is larger. In the Southern Hemisphere, the seasonal variability amplitude is much smaller at 0.3 ppm, thus lowering the correlation coefficient.

The comparisons in this section indicate that, in general, geographical colocation has low matching yield and poor accuracy performance. This is likely because the geographical colocation used (same-day 500 km circle) lacks the large coincident neighborhood to reduce the individual retrieval variability through averaging. Wunch et al.'s (2011) T_{700} and geostatistical colocation both take advantage of a larger colocation neighborhood to produce more accurate ACOS-GOSAT colocated values.

While these methodologies produce roughly the same bias estimates, geostatistical colocation produces distinctly lower RMSE. This improvement likely comes from the fact that while the existing colocation methodologies tend to give equal weights to all satellite observations falling within the coincident window, our methodology gives different weights to the coincident satellite observations based on the distance metric defined in Eq. (10). X_{CO_2} in general tends to be a smoothly varying field and it can be reasonably assumed to follow the geographical principle that locations close to one another are more likely to be similar than locations far apart (Tobler, 1970); therefore our methodology produces better accuracy because its spatial-dependency model is more reflective and representative of the true underlying X_{CO_2} field.

5 Conclusions

Validation colocation, or the practice of interpolating satellite and ground-based validation data to the same spatiotemporal coordinate, is an important part of instrument validation and assessment. All colocation methodologies are essentially data interpolation, which carries with it interpolation error. This interpolation error is an extra component in the RMSE
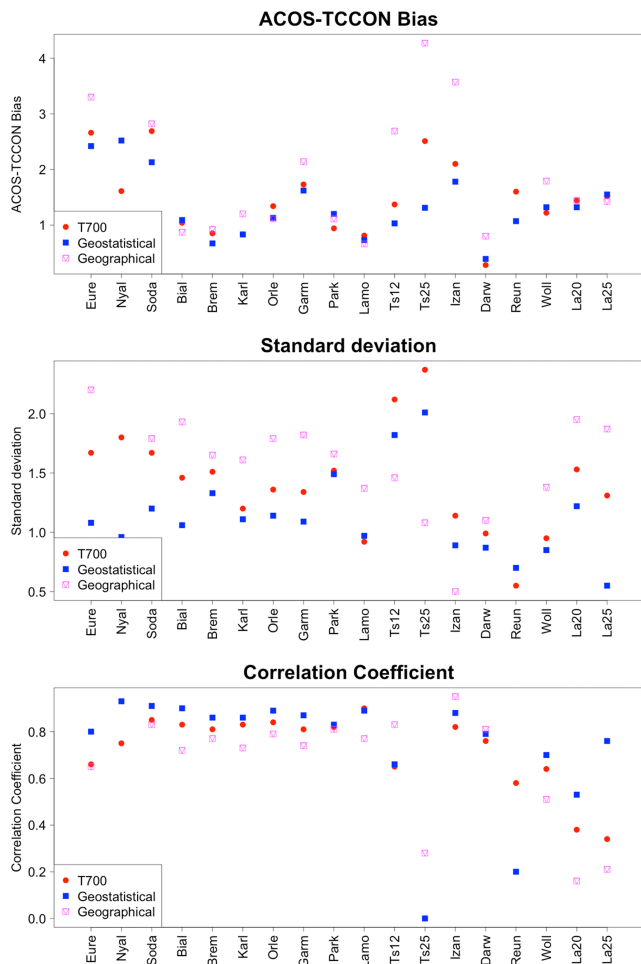
Figure 5. Summary statistics for the comparison between ACOS and TCCON using three colocation methodologies (top panel: bias; middle panel: standard deviation; bottom panel: correlation coefficients). TCCON stations are listed in order of decreasing latitude.

of the difference between validation and colocated data; it is important to minimize the interpolation error as much as possible in order to better assess important instrumental and operational metrics such as bias and variability relative to the validation data.

This paper examines a new colocation technique in comparing ACOS-GOSAT and TCCON data. We model the spatial dependence structure as being isotropic under a modified Euclidean distance metric. Our methodology is similar to previous colocation techniques (e.g., geographical, T_{700}, model-based) in that we assume that nearby observations are more likely to be correlated than observations far apart. However, whereas the existing methodologies define some neighborhood regions and then give all neighboring observations equal weights, our methodology weights each observation depending on the distances between the data and the interpolation location of interest.

In Sect. 4, we show that our geostatistical colocation methodology has the lowest mean-squared error of the difference between colocated ACOS-GOSAT data and TCCON data when compared with two existing colocation methodologies. Naturally, one would expect the correlation structure in ACOS-GOSAT X_{CO_2} to vary *smoothly* as a function of distance, and hence our method has better performance because its spatial correlation model is more approximate to the true underlying spatial structure. While we applied the methodology in Sect. 3 to ACOS-GOSAT and TCCON data, the colocation methodology can be readily applied to other satellite instruments and other geophysical processes where the underlying correlation structure can be reasonably assumed to vary smoothly as a function of distance.

In Sect. 3, we chose to use midtropospheric temperature as a covariate to improve our interpolation; it is possible to replace T_{700} with another covariate such as 3-day-averaged model X_{CO_2} as in the model-based method. While the parameters of the resulting correlation function would change with the replacement of T_{700}, the parameter estimation procedure in Sect. 3.3 would remain the same. We also note that the distance metric we derived in Eq. (10) has value beyond performing geostatistical colocation. It could be used as a stand-alone metric in assessing proximity (e.g., finding k-nearest neighbors, computing inverse distance weighting, constructing Voronoi diagrams, etc.).

In this paper we assumed that ACOS-GOSAT retrievals can be approximated and treated as zero-area points. In certain applications it may be more reasonable to assume that a satellite observation is an average of the true geophysical process $Y(\cdot)$ over the area of the footprint plus a measurement-error term. The resulting process of inferring a spatial process at one resolution from data at another resolution, also known as the change-of-support problem, is more complex; see Gotway and Young (2002) for a review. In general, there is no analytical solution for estimating the parameters of standard variogram models from areal data (e.g., spherical, exponential, etc.); however, certain classes of spatial models provide for straightforward and seamless parameter estimation (for instance, see spatial random effects model; Cressie and Johannesson, 2008; Nguyen et al., 2012).

In Sect. 4, we model the variogram parameters as temporally constant. An extension of the methodology would be to model temporal dependence in the variogram parameters. Naturally, good models of the temporal dependence would improve the colocation performance, but there is a trade-off in the complexity of the temporal evolution models and the robustness of the parameter estimates. One possible approach would be to assume that the spatial-correlation structure is constant over a season, although care would be needed in combining data straddling different seasons. Further examination of the trade-off between estimation robustness and temporal evolution complexity would be needed.

References

ACOS Data Access: Goddard Earth Sciences Data and Information Services Center, available at: http://disc.sci.gsfc.nasa.gov/acdisc/documentation/ACOS.shtml, last access: June 2013.

Artis, M., Clavel, J. G., Hoffmann, M., and Nachane, D.: Harmonic Regression Models: A Comparative Review with Applications, IEW – Working Papers 333, Institute for Empirical Research in Economics – University of Zurich, 2007.

Boesch, H., Baker, D., Connor, B., Crisp, D., and Miller, C.: Global Characterization of CO_2 Column Retrievals from Shortwave-Infrared Satellite Observations of the Orbiting Carbon Observatory-2 Mission, Remote Sensing, 3, 270–304, 2011.

Bosch, H., Toon, G. C., Sen, B., Washenfelder, R. A., Wennberg, P. O., Buchwitz, M., de Beek, R., Burrows, J. P., Crisp, D., Christi, M., Connor, B. J., Natraj, V., and Yung, Y. L.: Space-based near-infrared CO_2 measurements: Testing the Orbiting Carbon Observatory retrieval algorithm and validation concept using SCIAMACHY observations over Park Falls, Wisconsin, J. Geophys. Res. Atmos., 111, D23302, doi:10.1029/2006JD007080, 2006.

Bovensmann, H., Burrows, J., Buchwitz, M., Frederick, J., Noel, S., Rozanov, V. V., Chance, K. V., and Geode, A. P. H.: SCIAMACHY: Mission objectives and measurement modes, J. Atmos. Sci., 56, 127–150, 1999.

Butz, A., Guerlet, S., Jacob, D. J., Schepers, D., Galli, A., Aben, I., Frankenberg, C., Hartmann, J.-M., Tran, H., Kuze, A., Keppel-Aleks, G., Toon, G. C., Wunch, D., Wennberg, P. O., Deutscher, N. M., Griffith, D. W. T., Macatangay, R., Messerschmidt, J., Notholt, J., and Warneke, T.: Toward accurate CO_2 and CH_4 observations from GOSAT, Geophys. Res. Lett., 38, 2–7, 2011.

Cogan, A. J., Boesch, H., Parker, R. J., Feng, L., Palmer, P. I., Blavier, J.-F. L., Deutscher, N. M., Macatangay, R., Notholt, J., Roehl, C., Warneke, T., and Wunch, D.: Atmospheric carbon dioxide retrieved from the Greenhouse gases Observing SATellite (GOSAT): Comparison with ground-based TCCON observations and GEOS-Chem model calculations, J. Geophys. Res. Atmos., 117, D21301, doi:10.1029/2012JD018087, 2012.

Connor, B. J., Boesch, H., Toon, G., Sen, B., Miller, C., and Crisp, D.: Orbiting Carbon Observatory: Inverse method and prospective error analysis, J. Geophys. Res. Atmos., 113, D05305, doi:10.1029/2006JD008336, 2008.

Cressie, N.: M-estimation in the presence of unequal scale, Statistica Neerlandica, 34, 19–32, 1980.

Cressie, N.: Fitting Variogram Models by Weighted Least Squares, Mathematical Geology, 17, 563–570, 1985.

Cressie, N.: Statistics for Spatial Data, revised edition, Wiley-Interscience, New York, NY, 1993.

Cressie, N. and Johannesson, G.: Fixed rank kriging for very large spatial data sets, J. Roy. Stat. Soc. Ser. B, 70, 209–226, 2008.

Crisp, D., Fisher, B. M., O'Dell, C., Frankenberg, C., Basilio, R., Bösch, H., Brown, L. R., Castano, R., Connor, B., Deutscher, N. M., Eldering, A., Griffith, D., Gunson, M., Kuze, A., Mandrake, L., McDuffie, J., Messerschmidt, J., Miller, C. E., Morino, I., Natraj, V., Notholt, J., O'Brien, D. M., Oyafuso, F., Polonsky, I., Robinson, J., Salawitch, R., Sherlock, V., Smyth, M., Suto, H., Taylor, T. E., Thompson, D. R., Wennberg, P. O., Wunch, D., and Yung, Y. L.: The ACOS CO_2 retrieval algorithm – Part II: Global XCO_2 data characterization, Atmos. Meas. Tech., 5, 687—707, doi:10.5194/amt-5-687-2012, 2012.

Deutscher, N. M., Griffith, D. W. T., Bryant, G. W., Wennberg, P. O., Toon, G. C., Washenfelder, R. A., Keppel-Aleks, G., Wunch, D., Yavin, Y., Allen, N. T., Blavier, J.-F., Jiménez, R., Daube, B. C., Bright, A. V., Matross, D. M., Wofsy, S. C., and Park, S.: Total column CO_2 measurements at Darwin, Australia – site description and calibration against in situ aircraft profiles, Atmos. Meas. Tech., 3, 947–958, doi:10.5194/amt-3-947-2010, 2010.

Gotway, C. A. and Young, L. J.: Combining Incompatible Spatial Data, J. Am. Stat. Assoc., 97, 632–648, 2002.

Gruber, N., Gloor, M., Fletcher, S. E. M., Dutkiewicz, S., Follows, M., Doney, S. C., Gerber, M., Jacobson, A. R., Lindsay, K., Menemenlis, D., Mouchet, A., Mueller, S. A., Sarmiento, J. L., and Takahashi, T.: Oceanic sources, sinks, and transport of atmospheric CO2, Global Biogeochem. Cy., 23, GB1005, doi:10.1029/2008GB003349, 2009.

Guerlet, S., Butz, A., Schepers, D., Basu, S., Hasekamp, O. P., Kuze, A., Yokota, T., Blavier, J.-F., Deutscher, N. M., Griffith, D. W., Hase, F., Kyro, E., Morino, I., Sherlock, V., Sussmann, R., Galli, A., and Aben, I.: Impact of aerosol and thin cirrus on retrieving and validating XCO2 from GOSAT shortwave infrared measurements, J. Geophys. Res. Atmos., 118, 4887–4905, 2013.

Hamazaki, T., Kaneko, Y., Kuze, A., and Kondo, K.: Fourier transform spectrometer for Greenhouse Gases Observing Satellite (GOSAT), in: Society of Photo-Optical Instrumentation Engineers (SPIE) Conference Series, edited by: Komar, G. J., Wang, J., and Kimura, T., vol. 5659 of Society of Photo-Optical Instrumentation Engineers (SPIE) Conference Series, 73–80, 2005.

Inoue, M., Morino, I., Uchino, O., Miyamoto, Y., Yoshida, Y., Yokota, T., Machida, T., Sawa, Y., Matsueda, H., Sweeney, C., Tans, P. P., Andrews, A. E., Biraud, S. C., Tanaka, T., Kawakami, S., and Patra, P. K.: Validation of XCO_2 derived from SWIR spectra of GOSAT TANSO-FTS with aircraft measurement data, Atmos. Chem. Phys., 13, 9771–9788, doi:10.5194/acp-13-9771-2013, 2013.

Kalnay, E., Kanamitsu, M., Kistler, R., Collins, W., Deaven, D., Gandin, L., Iredell, M., Saha, S., White, G., Woollen, J., Zhu, Y., Leetmaa, A., and Reynolds, R.: The NCEP/NCAR 40-Year Reanalysis Project, Bull. Am. Meteorol. Soc., 77, 437–471, 1996.

Keppel-Aleks, G., Wennberg, P. O., and Schneider, T.: Sources of variations in total column carbon dioxide, Atmos. Chem. Phys., 11, 3581–3593, doi:10.5194/acp-11-3581-2011, 2011.

Keppel-Aleks, G., Wennberg, P. O., Washenfelder, R. A., Wunch, D., Schneider, T., Toon, G. C., Andres, R. J., Blavier, J.-F., Con-

nor, B., Davis, K. J., Desai, A. R., Messerschmidt, J., Notholt, J., Roehl, C. M., Sherlock, V., Stephens, B. B., Vay, S. A., and Wofsy, S. C.: The imprint of surface fluxes and transport on variations in total column carbon dioxide, Biogeosciences, 9, 875–891, doi:10.5194/bg-9-875-2012, 2012.

Messerschmidt, J., Geibel, M. C., Blumenstock, T., Chen, H., Deutscher, N. M., Engel, A., Feist, D. G., Gerbig, C., Gisi, M., Hase, F., Katrynski, K., Kolle, O., Lavrič, J. V., Notholt, J., Palm, M., Ramonet, M., Rettinger, M., Schmidt, M., Sussmann, R., Toon, G. C., Truong, F., Warneke, T., Wennberg, P. O., Wunch, D., and Xueref-Remy, I.: Calibration of TCCON column-averaged CO_2: the first aircraft campaign over European TCCON sites, Atmos. Chem. Phys., 11, 10765–10777, doi:10.5194/acp-11-10765-2011, 2011.

Morino, I., Uchino, O., Inoue, M., Yoshida, Y., Yokota, T., Wennberg, P. O., Toon, G. C., Wunch, D., Roehl, C. M., Notholt, J., Warneke, T., Messerschmidt, J., Griffith, D. W. T., Deutscher, N. M., Sherlock, V., Connor, B., Robinson, J., Sussmann, R., and Rettinger, M.: Preliminary validation of column-averaged volume mixing ratios of carbon dioxide and methane retrieved from GOSAT short-wavelength infrared spectra, Atmos. Meas. Tech., 4, 1061–1076, doi:10.5194/amt-4-1061-2011, 2011.

Nguyen, H., Cressie, N., and Braverman, A.: Spatial statistical data fusion for remote sensing applications, J. Am. Stat. Assoc., 107, 1004–1018, 2012.

O'Dell, C. W., Connor, B., Bösch, H., O'Brien, D., Frankenberg, C., Castano, R., Christi, M., Eldering, D., Fisher, B., Gunson, M., McDuffie, J., Miller, C. E., Natraj, V., Oyafuso, F., Polonsky, I., Smyth, M., Taylor, T., Toon, G. C., Wennberg, P. O., and Wunch, D.: The ACOS CO_2 retrieval algorithm – Part 1: Description and validation against synthetic observations, Atmos. Meas. Tech., 5, 99–121, doi:10.5194/amt-5-99-2012, 2012.

Oshchepkov, S., Bril, A., Yokota, T., Morino, I., Yoshida, Y., Matsunaga, T., Belikov, D., Wunch, D., Wennberg, P. O., Toon, G. C., O'Dell, C. W., Butz, A., Guerlet, S., Cogan, A., Boesch, H., Eguchi, N., Deutscher, N. M., Griffith, D., Macatangay, R., Notholt, J., Sussmann, R., Rettinger, M., Sherlock, V., Robinson, J., Kyrö, E., Heikkinen, P., Feist, D. G., Nagahama, T., Kadygrov, N., Maksyutov, S., Uchino, O., and Watanabe, H.: Effects of atmospheric light scattering on spectroscopic observations of greenhouse gases from space: Validation of PPDF-based CO2 retrievals from GOSAT, J. Geophys. Res., 117, 1–18, 2012.

Osterman, G., Eldering, A., Avis, C., O'Dell, C., Martinez, E., Frankenberg, C., Fisher, B., and Wunch, D.: ACOS Level 2 Standard Product Data User's Guide v3.3, Revision Date: Revision G, 13 June 2013, available at: http://oco.jpl.nasa.gov/files/oco/ACOS_v3.3_DataUsersGuide.pdf, 2013.

Peters, W., Jacobson, A. R., Sweeney, C., Andrews, A. E., Conway, T. J., Masarie, K., Miller, J. B., Bruhwiler, L. M. P., Pétron, G., Hirsch, A. I., Worthy, D. E. J., van der Werf, G. R., Randerson, J. T., Wennberg, P. O., Krol, M. C., and Tans, P. P.: An atmospheric perspective on North American carbon dioxide exchange: CarbonTracker, Proc. Natl. Aca. Sci., 104, 18925–18930, 2007.

Reuter, M., Bösch, H., Bovensmann, H., Bril, A., Buchwitz, M., Butz, A., Burrows, J. P., O'Dell, C. W., Guerlet, S., Hasekamp, O., Heymann, J., Kikuchi, N., Oshchepkov, S., Parker, R., Pfeifer, S., Schneising, O., Yokota, T., and Yoshida, Y.: A joint effort to deliver satellite retrieved atmospheric CO_2 concentrations for

surface flux inversions: the ensemble median algorithm EMMA, Atmos. Chem. Phys., 13, 1771–1780, doi:10.5194/acp-13-1771-2013, 2013.

Rodgers, C. D.: Inverse methods for atmospheric sounding: theory and practice, vol. 2 of Series on atmospheric, oceanic and planetary physics, World Scientific, River Edge, N.J., 2000.

Rodgers, C. D. and Connor, B. J.: Intercomparison of remote sounding instruments, J. Geophys. Res. Atmos., 108, 4116, doi:10.1029/2002JD002299, 2003.

TCCON Data Access: TCCON Data Archive, available at: http://tccon.ipac.caltech.edu/, recommended bias corrections: https://tccon-wiki.caltech.edu/Network_Policy/Data_Use_Policy/Data_Description#Laser_Sampling_Errors, last access: June 2013.

Tobler, W.: A computer movie simulating urban growth in the Detroit region, Economic Geography, 46, 234–240, 1970.

Washenfelder, R. A., Toon, G. C., Blavier, J.-F., Yang, Z., Allen, N. T., Wennberg, P. O., Vay, S. A., Matross, D. M., and Daube, B. C.: Carbon dioxide column abundances at the Wisconsin Tall Tower site, J. Geophys. Res. Atmos., 111, D22305, doi:10.1029/2006JD007154, 2006.

Wunch, D., Toon, G. C., Wennberg, P. O., Wofsy, S. C., Stephens, B. B., Fischer, M. L., Uchino, O., Abshire, J. B., Bernath, P., Biraud, S. C., Blavier, J.-F. L., Boone, C., Bowman, K. P., Browell, E. V., Campos, T., Connor, B. J., Daube, B. C., Deutscher, N. M., Diao, M., Elkins, J. W., Gerbig, C., Gottlieb, E., Griffith, D. W. T., Hurst, D. F., Jiménez, R., Keppel-Aleks, G., Kort, E. A., Macatangay, R., Machida, T., Matsueda, H., Moore, F., Morino, I., Park, S., Robinson, J., Roehl, C. M., Sawa, Y., Sherlock, V., Sweeney, C., Tanaka, T., and Zondlo, M. A.: Calibration of the Total Carbon Column Observing Network using aircraft profile data, Atmos. Meas. Tech., 3, 1351—1362, doi:10.5194/amt-3-1351-2010, 2010.

Wunch, D., Toon, G., Blavier, J., Washenfelder, R., Notholt, J., Connor, B., Griffith, D., Sherlock, V., and Wennberg, P.: The Total Carbon Column Observing Network, Philos. Trans. Roy. Soc. A, 369, 2087–2112, 2011a.

Wunch, D., Wennberg, P. O., Toon, G. C., Connor, B. J., Fisher, B., Osterman, G. B., Frankenberg, C., Mandrake, L., O'Dell, C., Ahonen, P., Biraud, S. C., Castano, R., Cressie, N., Crisp, D., Deutscher, N. M., Eldering, A., Fisher, M. L., Griffith, D. W. T., Gunson, M., Heikkinen, P., Keppel-Aleks, G., Kyrö, E., Lindenmaier, R., Macatangay, R., Mendonca, J., Messerschmidt, J., Miller, C. E., Morino, I., Notholt, J., Oyafuso, F. A., Rettinger, M., Robinson, J., Roehl, C. M., Salawitch, R. J., Sherlock, V., Strong, K., Sussmann, R., Tanaka, T., Thompson, D. R., Uchino, O., Warneke, T., and Wofsy, S. C.: A method for evaluating bias in global measurements of CO_2 total columns from space, Atmos. Chem. Phys., 11, 12317–12337, doi:10.5194/acp-11-12317-2011, 2011b.

Yokota, T., Oguma, H., I., M., and Inoue, G.: A nadir looking SWIR FTS to monitor CO2 column density for Japanese GOSAT project, Proc. Twenty-fourth Int. Sympo. on Space Technol. and Sci. (Selected Papers), 887–889, 2004.

Zeng, Z., Lei, L., Hou, S., Ru, F., Guan, X., and Zhang, B.: A Regional Gap-Filling Method Based on Spatiotemporal Variogram Model of CO2 Columns, IEEE Trans. Geosci. Remote Sens., 52, 3594–3603, 2014.